# On the autoxidation of terpenes: Detection of oxygenated and aromatic products

Zahraa Dbouk, Nesrine Belhadj, Maxence Lailliau, Roland Benoit, Philippe Dagaut

# On the autoxidation of terpenes: detection of oxygenated and aromatic products.

Zahraa Dbouk[a,b], Nesrine Belhadj[a,b], Maxence Lailliau[a,b], Roland Benoit[a], Philippe Dagaut[a]

[a] *C.N.R.S., 1C Avenue de la Recherche Scientifique, Orléans, 45071, France*

[b] *Université d'Orléans, Avenue de Parc Floral, Orléans, 45067, France*

**Correspondence**: philippe.dagaut@cnrs-orleans.fr

**Keywords**: terpene, limonene, α-pinene, oxidation, cool flame, jet-stirred reactor, Orbitrap

**Highlights**:

- Stable products of oxidation measured by FTIR
- Ketohydroperoxides were detected by Orbitrap
- Highly oxidized products were detected by Orbitrap
- Highly unsaturated products were detected by Orbitrap
- Products of Korcek and Waddington mechanisms detected

**Abstract**

Limonene-$O_2$-$N_2$ and α-pinene-$O_2$-$N_2$ mixtures were oxidized in a jet-stirred reactor at atmospheric pressure, in the cool flame regime, and fuel-lean conditions. Samples of the reacting mixtures were analyzed by on-line Fourier transform infrared (FTIR) and collected, dissolved in acetonitrile for analysis by flow injection or chromatographic separation by ultra-high performance liquid chromatography and Orbitrap mass spectrometry. OH/OD exchange using $D_2O$ and reaction with 2,4-dinitrophenylhydrazine were carried out for probing the existence of hydroxyl or hydroperoxyl, and carbonyl functions in the products, respectively. A large number of oxidation products, including highly oxygenated organic products with more than ten oxygen atoms, were observed. Unexpectedly, aromatic and polyunsaturated products with a contribution of 8-10% were detected for both terpenes over the range of temperatures studied. Van Krevelen plots, computed oxidation state of carbon, aromaticity index, and aromaticity equivalent index in products were used to rationalize the results.

## 1. Introduction

The terpenes are naturally released by vegetation. They constitute a large fraction of volatile organic chemicals detected in the troposphere [1]. Besides, because of their high-energy-density, they could be used as biojet fuels [2, 3]. With their high octane numbers (e.g., 88-89 for limonene [4, 5] and 84 for α-pinene [5]), one could also use them as drop-in fuels to reduce the carbon footprint in transportation.

However, the use of terpenes as biofuel or drop-in fuel would certainly contribute to increasing their concentration in the troposphere through unburnt fuel emissions and evaporation during transport and refueling. While the terpenes kinetics of oxidation under atmosphere-relevant conditions has been the topic of many works, a good understanding of the multiple oxidation routes has not been attained yet [6]. The chemical kinetics of combustion of such chemicals have not received much attention to date. Indeed, only burning velocity in air, impact on ignition, and flame structures have been reported [7-9]. This is not enough to characterize terpenes oxidation chemistry which involves many reaction pathways, particularly under cool flame conditions. In hydrocarbons (RH) cool flames, we consider the production of oxygenates such as ketohydroperoxides (KHPs) which lead to chain branching via decomposition [10]: RH + $^{\bullet}$OH → R$^{\bullet}$ + $H_2O$ (1), R$^{\bullet}$ + $O_2$ ⇄ $RO_2^{\bullet}$ (2), $RO_2^{\bullet}$ + $HO_2^{\bullet}$ ⇄ $RO_2H$ + $O_2$ (3), $RO_2^{\bullet}$ + RH ⇄ $RO_2H$ + R$^{\bullet}$ (4), $RO_2^{\bullet}$ ⇄ $^{\bullet}QO_2H$ (5), $RO_2^{\bullet}$ ⇄ Q (unsaturated product) + $HO_2^{\bullet}$ (6), $^{\bullet}QO_2H$ ⇄ $^{\bullet}$OH + QO (cyclic ether) (7), $^{\bullet}QO_2H$ + $O_2$ ⇄ $^{\bullet}OOQO_2H$ (8), $^{\bullet}O_2QO_2H$ ⇄ $HO_2{}^{\bullet}PO_2H$ (9), $HO_2{}^{\bullet}PO_2H$ ⇄ $^{\bullet}$OH + $HO_2P$=O (KHPs) (10), $HO_2P$=O ⇄ $^{\bullet}$OH + OP$^{\bullet}$O (11). But, products of cool flame oxidation must be better characterized. Indeed, recent studies [11, 12] have demonstrated the formation of more oxygenated products in cool flames of a large set of fuels including *n*- and *iso*-alkanes, cycloalkanes, alcohols, aldehydes, esters, and ethers. There, alternative oxidation pathways proceed via an internal H-atom transfer in the $^{\bullet}O_2QO_2H$ intermediate, involving a H–C group other than the H–COOH group which is responsible for KHPs formation (Reactions 9 and 10). It opens new oxidation paths such as a third $O_2$ addition to $HO_2{}^{\bullet}PO_2H$ yielding $^{\bullet}O_2P(O_2H)_2$. Such sequence of H-transfer and $O_2$ addition can repeat several times, yielding highly oxidized products. Besides, $^{\bullet}QO_2H$ decomposition yields stable products and radicals via Reaction (7), $^{\bullet}QO_2H$ → olefin + carbonyl + $^{\bullet}$OH (12), and $^{\bullet}QO_2H$ → $HO_2^{\bullet}$ + olefin (13). In the case of unsaturated reactants, such as terpenes, in addition to these reaction pathways, the Waddington mechanism [13] can proceed. It starts via an $^{\bullet}$OH addition on a C=C double bond and continues with an $O_2$ addition and H-atom internal transfer from the hydroxyl group formed in Reaction (14), to the peroxyl group via Reaction (16), followed by decomposition (Reaction 17): $R^1$–C=C–$R^2$ + $^{\bullet}$OH ⇄ $R^1$–$^{\bullet}$C–C(–$R^2$) –OH (14), $^{\bullet}$C(–$R^1$)–C(–$R^2$)–OH + $O_2$ ⇄ $^{\bullet}$OO–C(–$R^1$)–C(–$R^2$)–OH (15), $^{\bullet}$OO–C(–$R^1$)–C(–$R^2$)–OH ⇄ HOO–C(–$R^1$)–C($R^2$)–O$^{\bullet}$ (16), HOO–C(–$R^1$)–C($R^2$)–O$^{\bullet}$ → $R^1$–C=O + $R^2$–C=O + $^{\bullet}$OH (17). Via this sequence of reactions, the hydroxyl radical initially consumed in Reaction (14) is finally regenerated in Reaction (17).

The Korcek mechanism [13] can also occur. This reaction pathway transforms γ-ketohydroperoxides into a carbonyl product and a carboxylic acid. The Korcek mechanism has been considered in recent combustion modeling [14-16]. Besides, the potential formation of highly unsaturated or aromatic products from the oxidation of monoterpenes has not received attention, but needs to be investigated.

In this work, our goal is to provide a better characterization of the products of autoxidation of two terpenes, namely limonene and α-pinene, under cool-flame conditions, and to investigate the formation

of highly unsaturated or aromatic products there. To this end, we carried out oxidation experiments in a jet-stirred reactor at 1 bar, and oxidation products were characterized using high-resolution mass spectrometry (Orbitrap HRMS). The complexity and size of datasets generated by HRMS require the use of visualization tools to interpret the data. Here, Van Krevelen plots [17], oxidation state of carbon [18], aromaticity index [19], and aromaticity equivalent index [20] were used.

## 2. Experiment

### *2.1 Oxidation experiments*

Experiments were conducted in a 42 mL fused silica jet-stirred-reactor (JSR) introduced earlier [21, 22]. As previously [23, 24] for the injection of the fuels (98 % pure), we utilized a HPLC pump with an online degasser. The fuels were sent to an in-house atomizer-vaporizer assembly fed with a nitrogen flow. Fuel-$N_2$ (99.95 % pure) and $N_2$-$O_2$ (99.995 % pure) were carried separately to the reactor to avoid premature oxidation before reaching the JSR entrance. Mass flow meters were used to deliver the nitrogen and oxygen flows. A fused silica protected thermocouple (0.1 mm Pt-Pt/Rh-10% wires) was moved along the vertical axis of the JSR to check thermal homogeneity. Typical gradients of < 1 K/cm were measured. To study the oxidation of the fuels in the cool-flame regime (520-680 K), we used 1% of fuel and operated at 1 bar, in fuel-lean conditions ($\varphi = 0.5$), and at 1.5 s mean residence time.

### *2.2 Chemical analyses*

Low-temperature oxidation products were dissolved into 20 mL of ≥ 99.9 pure acetonitrile, maintained at 273 K, through 60 min bubbling. They were stored in a freezer at 258 K for the next chemical analyses. Flow injection analyses/heated electrospray ionization (FIA/HESI) were done. The samples were analyzed by Orbitrap Q-Exactive. Several *m/z* ranges were used for data acquisition in order to improve C-trap transmission sensitivity [25]: 50-750, 150-750, and 300-750. Only signal ≥ 5000 counts were considered here. We performed mass calibrations in positive and negative ionization modes using +/– HESI calibration mixtures. Reverse-phase ultra-high-performance liquid chromatography (RP-UHPLC) analyses were performed using a C18 chromatographic column (1.6µm, 100 Å, 100x2.1 mm, Phenomenex Luna). 3 µL of samples were eluted by a water-acetonitrile (ACN) mix at a flow rate of 250 µL/min (gradient 5% to 90% ACN, during 33 min). Also, atmospheric pressure chemical ionization (APCI) was operated in positive and negative modes. Presently, with the techniques used in this work, no quantification could be made whereas, recent work addressed this issue using other experimental methods [26].

For determining the chemical structure of oxidation products after RP-UHPLC separation, MS/MS analyses were performed using the lowest collision cell energy (10 eV). As in preceding works [23, 24], 2,4-dinitrophenylhydrazine (2,4-DNPH) addition to samples was also used to assess the presence of carbonyl compounds. As before [11, 23, 24, 27], to evaluate the existence of hydroxyl (–OH) or hydroperoxyl (–OOH) groups in oxidation products, we performed H/D exchange by adding $D_2O$ to the samples. We analyzed these solutions using FIA-HESI-HRMS and RP-UHPLC-APCI-HRMS. For HRMS data, an uncertainty of ≤ 40% was estimated [23]. Besides, we performed online Fourier Transform Infrared spectroscopy (FTIR) analyses according to a procedure described in previous reports [16, 28]. FTIR measurements were made in the T-range 520-800 K and HRMS measurements in the T-range 540-680 K. Because gas samples have a complex composition, the infrared measurements of carbon dioxide mole fractions present uncertainties larger than usual. The validity of the measurement was checked carefully using the OMNIC and QuantPad softwares (ThermoScientific) and only reliable data are reported. Table S1 presents a summary of the analytical methods.

## 3. Results and discussion

### *3.1 Simple oxidation products and oxygenates*

Many oxidation products were detected during the oxidation of the two terpenes. Among them, simple products (not directly detectable by Orbitrap if they have a molecular weight <50) were measured by FTIR (Fig. 1). As can be seen from that figure, products mole fractions are similar for the two fuels. Formic acid was detected in FTIR analyses at small concentrations below 580 K for both fuels. We measured a maximum of 16 ± 10 ppm and 14 ± 10 ppm for α-pinene and limonene, respectively.

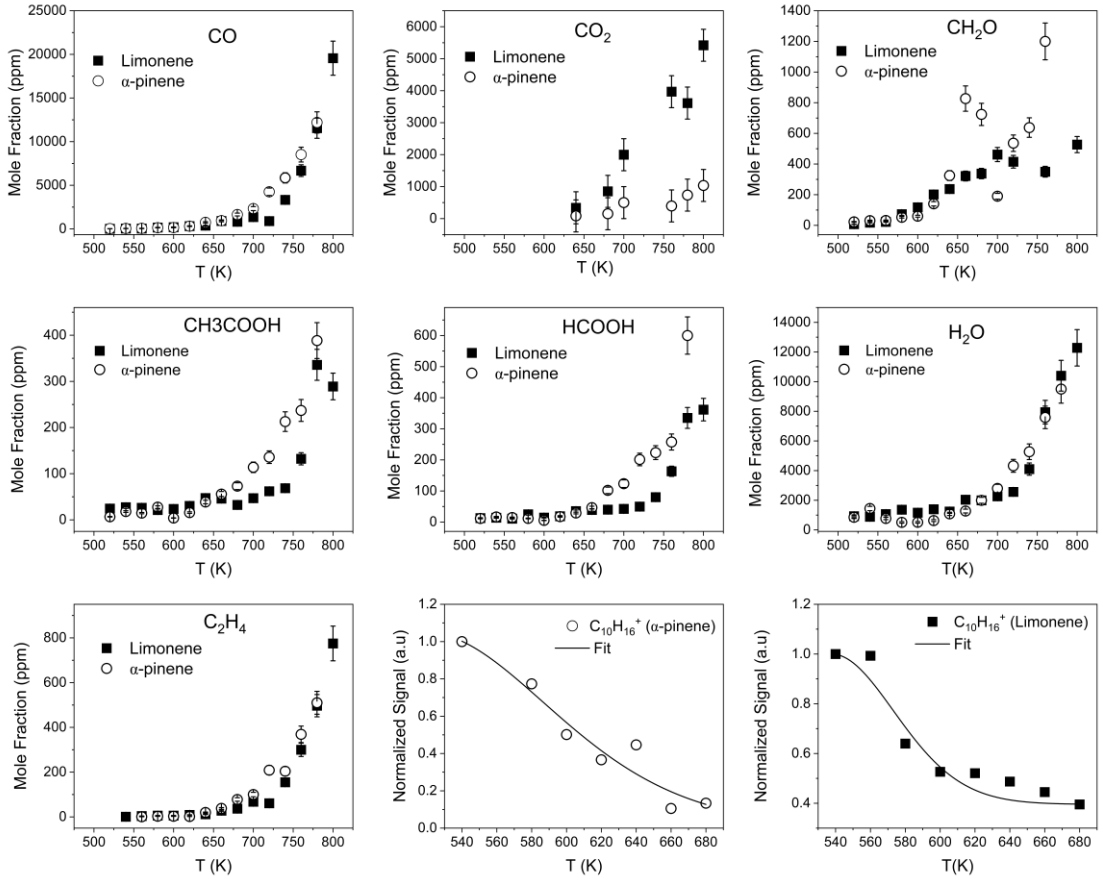


**Fig. 1.** Products measured during the oxidation of 1 % limonene and 1 % α-pinene in a JSR at 1 bar, equivalence ratio of 0.5 and residence time of 1.5 s, by FTIR and FIA-HESI(+)-HRMS (fuels).

A large set of chemical formulas was observed via HRMS analyses. The exact structures of chemical formulas cannot be determined precisely because of limitations in chromatographic separation of the very large set of chemicals. However, several tools (oxidation state of carbon, aromaticity index, and aromaticity equivalent index in products) were used to show the presence of several chemical classes in the products, as presented in the next paragraphs. Oxidation products containing O-atoms were detected in limonene oxidation products: $C_7H_{10}O_{4\text{ and }5}$, $C_8H_{12}O_{2\text{ and }4}$, $C_8H_{14}O_{2\text{ and }4}$, $C_9H_{12}O$, $C_9H_{14}O_{1\text{ and }3\text{ to }5}$, $C_{10}H_{12}O_2$, $C_{10}H_{14}O_{1\text{ to }9}$, $C_{10}H_{16}O_{2\text{ to }5}$, and $C_{10}H_{18}O_6$. For α-pinene oxidized under the same conditions, one could detect the following oxygenates: $C_7H_{10}O_{4\text{ and }5}$, $C_{10}H_{12}O_{2\text{ and }4}$, $C_{10}H_{14}O_{3\text{ and }5}$, $C_{10}H_{12}O_2$, $C_{10}H_{14}O_{1\text{ to }9}$, and $C_{10}H_{16}O_{2\text{ to }6}$. Figure 2 shows results obtained for KHPs and isomers and for diketones which result from KHPs decomposition. H/D exchange using $D_2O$ and reaction with 2,4-dinitrophenylhydrazine were performed to confirm the presence of hydroperoxyl, and carbonyl groups in the products, respectively. As can be seen from Figure 2, both products peak in the same range of temperature.

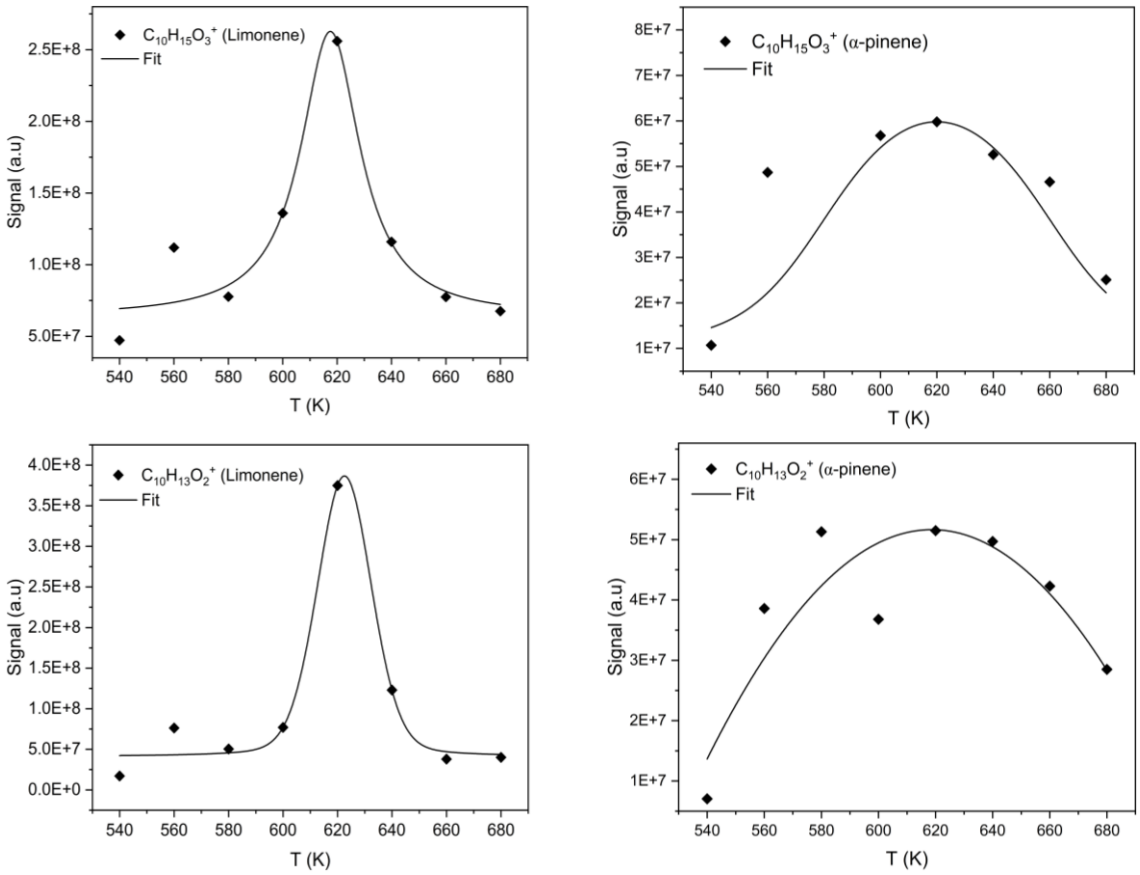


**Fig. 2.** Products of oxidation of limonene (left) and α-pinene (right) obtained by HRMS (symbols). The data for KHPs and isomers (top, $C_{10}H_{14}O_3$) and diketones and isomers (bottom, $C_{10}H_{12}O_2$) were obtained by FIA and HESI (+), i.e., $C_{10}H_{15}O_3^+$ *m/z* 183.1015 and $C_{10}H_{13}O_2^+$ *m/z* 165.0910, respectively. Errors estimated to be ±40%.

Carbonyl oxidation products formed through the Waddington mechanism on *exo*- and *endo*-double bonds (C=C) of limonene were observed ($C_9H_{14}O$, $C_{10}H_{16}O_2$) as well as products of their oxidation. In our previous study on the analysis of limonene oxidation products at atmospheric pressure [28], isoprenyl-6-oxoheptanal ($C_{10}H_{16}O_2$) was identified through the injection of a standard. While the characterization of limonaketone ($C_9H_{14}O$), produced via route (a) in Scheme 1, was based on the fragmentation spectrum in addition to the 2,4-DNPH derivatization. The RP-UHPLC-HRMS enabled the detection of several $C_9H_{14}O$ isomers ($C_9H_{15}O^+$, *m/z* 139.1117), as seen in Fig. S1. Almost all of these isomers react with 2,4-DNPH. A fragmentation mechanism was proposed for the limonaketone and is presented in Fig. S2. The resulting fragments were found in the MS/MS spectrum of the isomer eluted at a retention time of 15.83 min (Fig. S2). Consequently, we considered that limonaketone was eluted at this time.

Products of oxidation via the Waddington mechanism (Scheme 1, route c) were also detected for α-pinene ($C_{10}H_{16}O_2$).

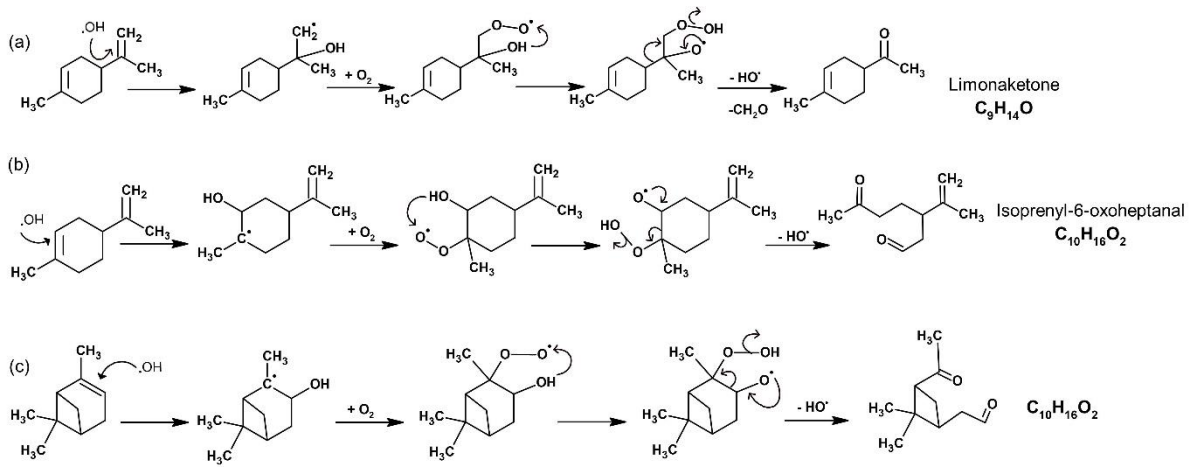


**Scheme 1.** Mechanism of oxidation of limonene (a) exo- and (b) endo-cyclic double bonds, and (c) α-pinene through the Waddington mechanism.

Earlier, it was reported [29] a higher reactivity of the *endo* double bond *vs*. the *exo* double bond. Estimated C-H bond dissociation energies, using a NREL software [30, 31], revealed a difference of 1.9 kcal/mol (the lower value found for the C-H in the *endo* double bond). Then, if H-atom abstraction on these C-H groups is of importance, that could partially explain the difference in reactivity of the two C-H groups. In line with the results presented earlier [29], higher ion signal was recorded for isoprenyl-6-oxoheptanal ($C_{10}H_{17}O_2^+$) than for limonaketone ($C_9H_{15}O^+$), which result from oxidation of *endo* and *exo* double bonds, respectively.

Oxidation products (carboxylic acids and carbonyls) formed via the Korcek mechanism were also detected (Fig. 3). For the two terpenes, the signal obtained for both formic acid and $C_9H_{12}O$ reach a maximum ~ 20 K higher than their parent ketohydroperoxides (see Fig. 2) which seems consistent with a formation of formic acid and $C_9H_{12}O$ via the Korcek mechanism.

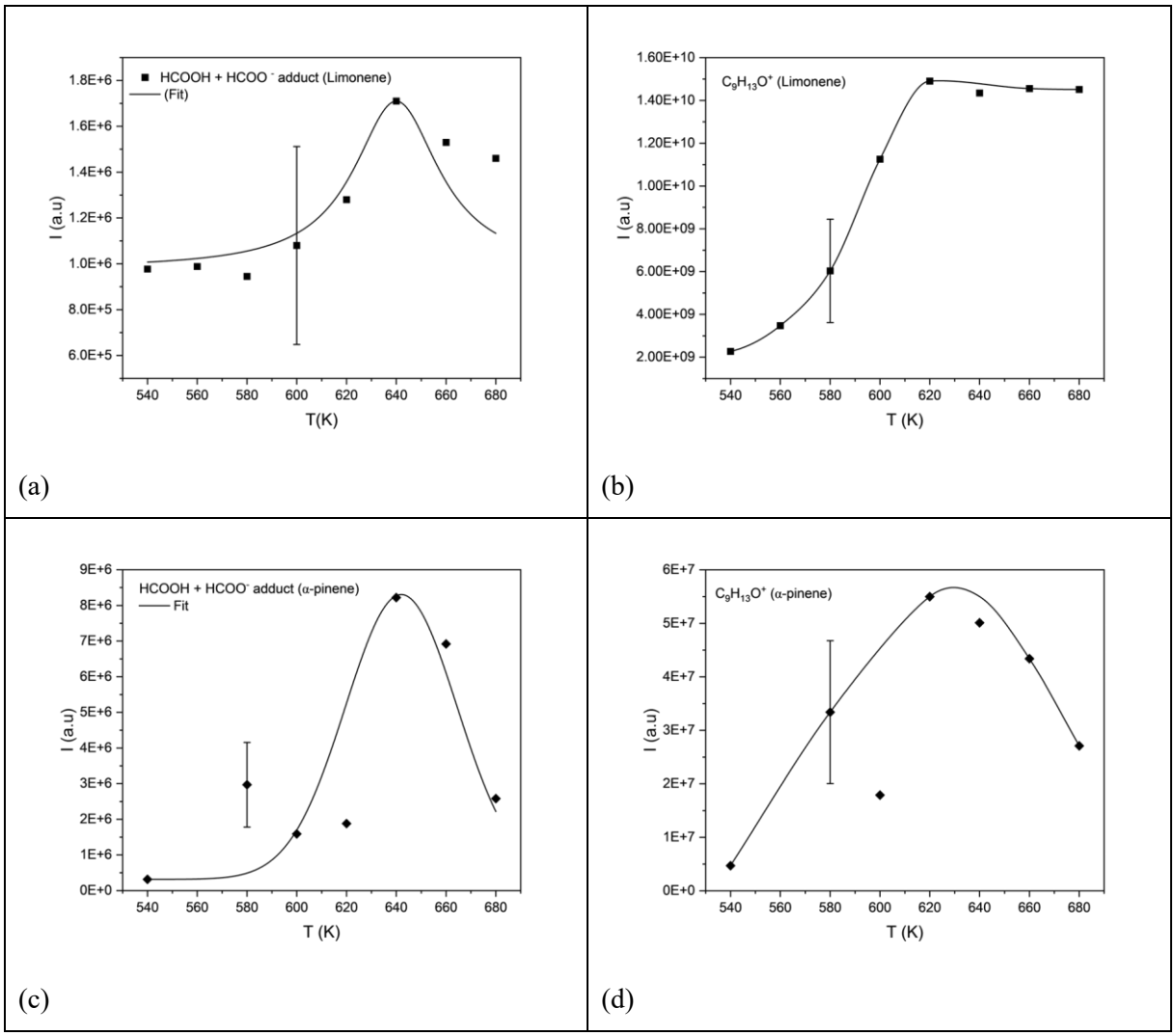


**Fig. 3**. Products of the Korcek mechanism during the oxidation of limonene and α-pinene. (a) and (b): data obtained by UHPLC-APCI(–) and UHPLC-APCI(+), respectively. (c) and (d): data obtained by FIA-HESI (–) and FIA-HESI(+), respectively. Errors estimated to be ±40%.

Among the 18 KHPs derived from limonene oxidation, four isomers could decompose via the Korcek mechanism. But, only one isomer can possibly yield a cyclic intermediate peroxide linking the carbonyl and OOH groups, which yields a carbonyl compound, $C_9H_{12}O$, and formic acid, $CH_2O_2$, by decomposition (Scheme 2). Both products were detected by UHPLC-HRMS in this study (Fig. 3). The three other KHPs isomers generated $C_{10}H_{14}O_3$ isomers.

As can be seen from Fig. S3 in the supplementary information, RP-UHPLC-HRMS enabled us to identify several $C_{10}H_{14}O_3$ isomers ($C_{10}H_{15}O_3^+$, *m/z* 183.1015).

After adding $D_2O$ to our sample, an intense H/D exchange ($C_{10}H_{14}D_1O_3^+$, *m/z* 184.1068, I= 1.25E+8) was detected indicating the presence of hydroperoxyl (OOH) or hydroxyl (OH) groups. At the same time, a signal corresponding to a second H/D exchange was detected ($C_{10}H_{13}D_2O_3^+$, *m/z* 185.1139, I=

5.22E+7) suggesting the presence of hydroxy-hydroperoxide isomers. Furthermore, confirmation of the presence of the C=O functional group was obtained through 2,4-DNPH derivatization. It should be noted that all $C_{10}H_{15}O_3^+$ isomers reacted with 2,4-DNPH, except that eluted at approximately 8.55 minutes, as shown in Fig. S4. This last product could be a hydroxy-hydroperoxide isomer.

In order to assess the presence of the products of the Korcek mechanism, the positive and negative modes of ionization / fragmentation spectra (MS/MS) of those isomers were used. It was confirmed that the specie produced by the decomposition of the KHPs isomer via route (b) in Scheme 2 was present in our sample.

One should note that in the fragmentation cell, the loss of $CO_2$ in negative mode from the parent ion $[M\text{-}H]^-$, as well as the loss of CO from the same ion, confirm the presence of an acidic function and an aldehyde group in the molecule, respectively [32, 33]. At a retention time of 6.9 min (Fig. S3), in addition to the fragments observed in positive mode and shown in Fig. S5, perfectly matching the structure of the suggested isomer, fragments corresponding to $[M\text{-}H\text{-}CO_2]^-$ ($C_9H_{13}O^-$, *m/z* 137.0961) and $[M\text{-}H\text{-}CO]^-$ ($C_9H_{13}O_2^-$, *m/z* 153.0909) were also detected in negative ionization mode (Fig. S6). These observations show that the isomer eluted at a retention time of 6.9 min contains acidic and aldehyde functions. The other products from the Korcek mechanism couldn't be identified.

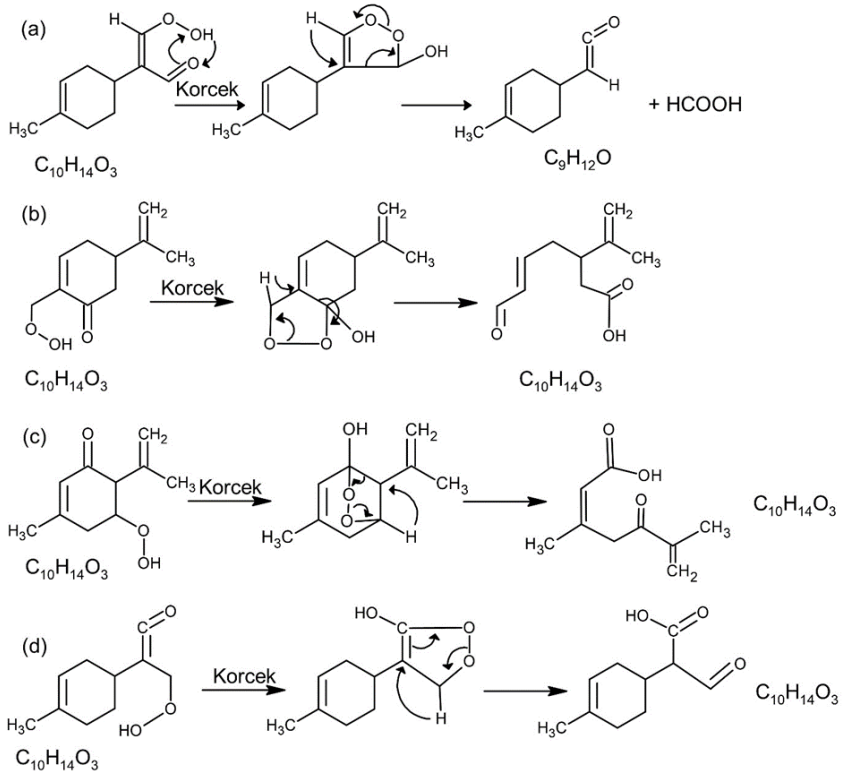


**Scheme 2**. Korcek mechanism during limonene oxidation.

For α-pinene, among the 22 KHPs derived from its oxidation, three isomers could decompose via the Korcek mechanism. Several products can be produced from these three γ-KHPs (Scheme 3). We tested

their presence in the products via FIA-HRMS. The products $C_9H_{12}O$ and $C_{10}H_{14}O_3$ (see Scheme 3) were detected by FIA-HRMS and UHPLC-HRMS. Unfortunately, MS/MS spectra did not allow us to identify the structure of the various oxidation products.

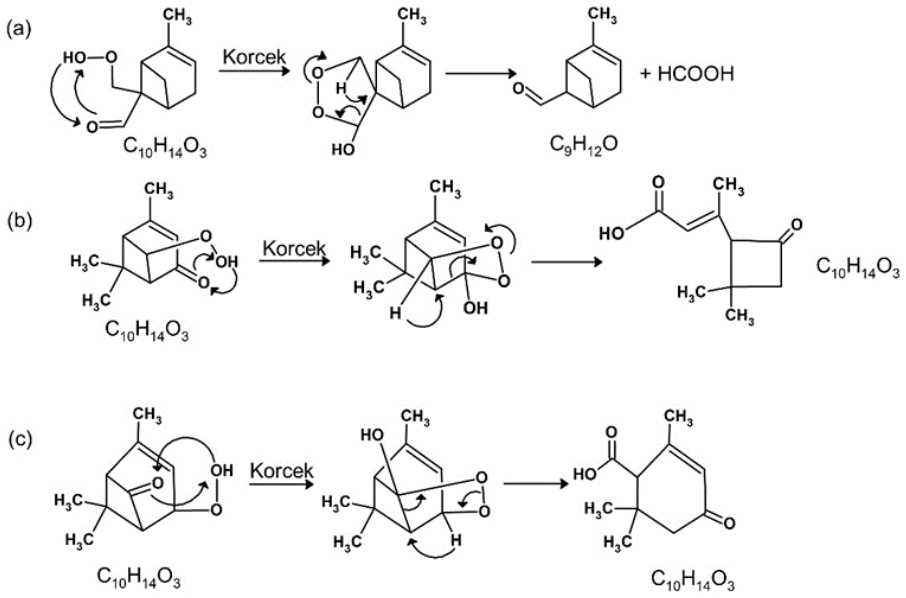


**Scheme 3**. Korcek mechanism during α-pinene oxidation.

Van Krevelen (VK) plots served to characterize the diversity of products of oxidation of limonene and α-pinene (Figs 4 and 5). As can be seen from these figures, similar products distribution was observed, although some differences could be noticed, as presented in the next Section. Also, one can see from these figures that many highly oxygenated species were formed, whereas products with no or little oxygen content were also detected (O/C = 0-0.1); see Section 3.2.

Limonene

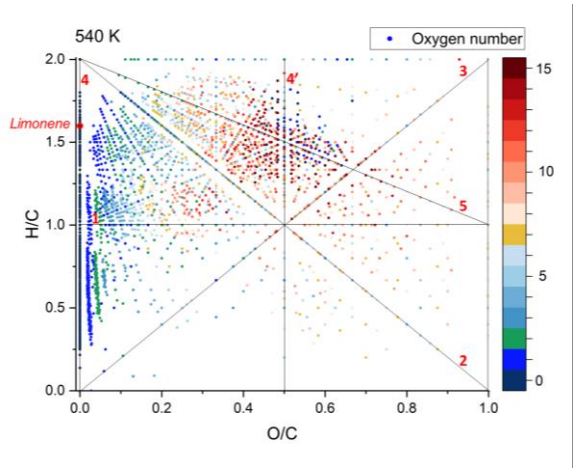


α-pinene

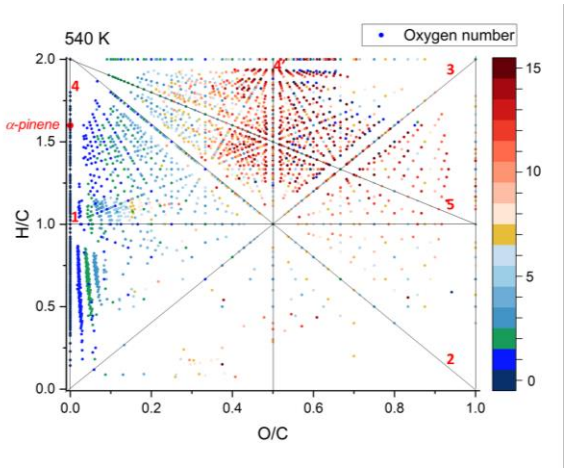

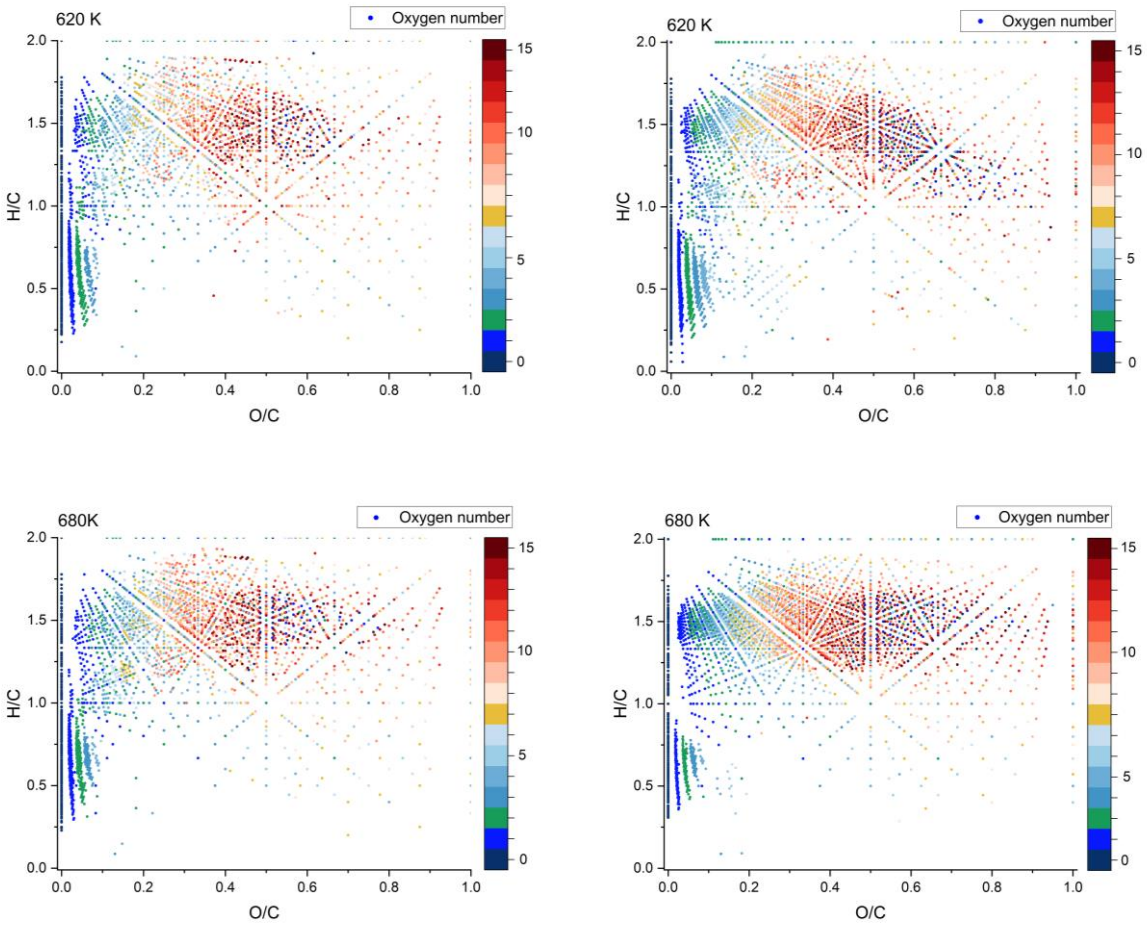


**Fig. 4.** Van Krevelen plot for limonene oxidation products (left) at three different temperatures (3025, 3199, and 3954 chemical formulas were detected at 540 K, 620 K, and 680 K, respectively). Van Krevelen plot for α-pinene oxidation products (right) at three different temperatures (2974, 4141, and 3361 chemical formulas were detected at 540 K, 620 K, and 680 K, respectively). 'Oxygen number' stands for number of oxygen atoms in chemical formulas.

HESI+/–, FIA-HRMS data were used to draw Fig. 4. The lines indicate different reaction paths, i.e., 1: oxidation, 2: carbonylation, 3: hydration, 4: dehydrogenation, 5: carboxylation, or reverse processes [34, 35]. Three temperatures (540, 620, and 680 K), among those studied, were chosen to characterize the oxidation of these two terpenes. They are visualized using Van Krevelen plots and OSc vs. number of carbon atoms graphs (Fig. 4 and Fig. 5, respectively). Here, OSc ≈ 2 O/C – H/C [16, 31] where H, C, and O represent the number of hydrogen, carbon, and oxygen atoms, respectively. Generally speaking, in the Van Krevelen graphs (Fig. 4), on line 5, around the point O/C=0.5 and H/C=1.5, we observe an increase in the number of chemical formulas associated with an increase in the number of O-atoms. Also, on line 1 (Fig. 4), we observe the formation of unsaturation (O/C=0, H/C<1) and the addition of oxygen to these unsaturated products (0<O/C<0.15 and H/C< 1). Although these oxidation phenomena occur

for both terpenes, the oxidation of α-pinene, in this temperature range, seems more advanced. The oxidation state of carbon, OSc was computed for the products of oxidation of the two fuels. The OSc versus the number of carbon atoms graphs (Fig. 5) confirm this observation and clarify the difference between these two terpenes. In the space defined by 10< C-atoms<40 and -2<OSc <3, the oxidation of α-pinene is more advanced in terms of H/C-O/C space size and level of oxidation (number of O-atoms in chemical formulas). By increasing temperature from 620 to 680 K, for α-pinene, chemical compounds with a number of C-atoms greater than 40 decreased by almost 50%, unlike in the case of limonene which was less affected (Fig. 5). This disappearance of chemical compounds belonging to the class of unsaturated or polyunsaturated compounds is concomitant with the development of the space 10 < number of C-atoms < 40 and -2 < OSc < 3 (Fig. 5). Different hypotheses, such as the opening of the ring and/or the presence of a double bond external to this ring in the case of limonene, will have to be further explored in order to understand the kinetics of oxidation specific to the two terpenes.

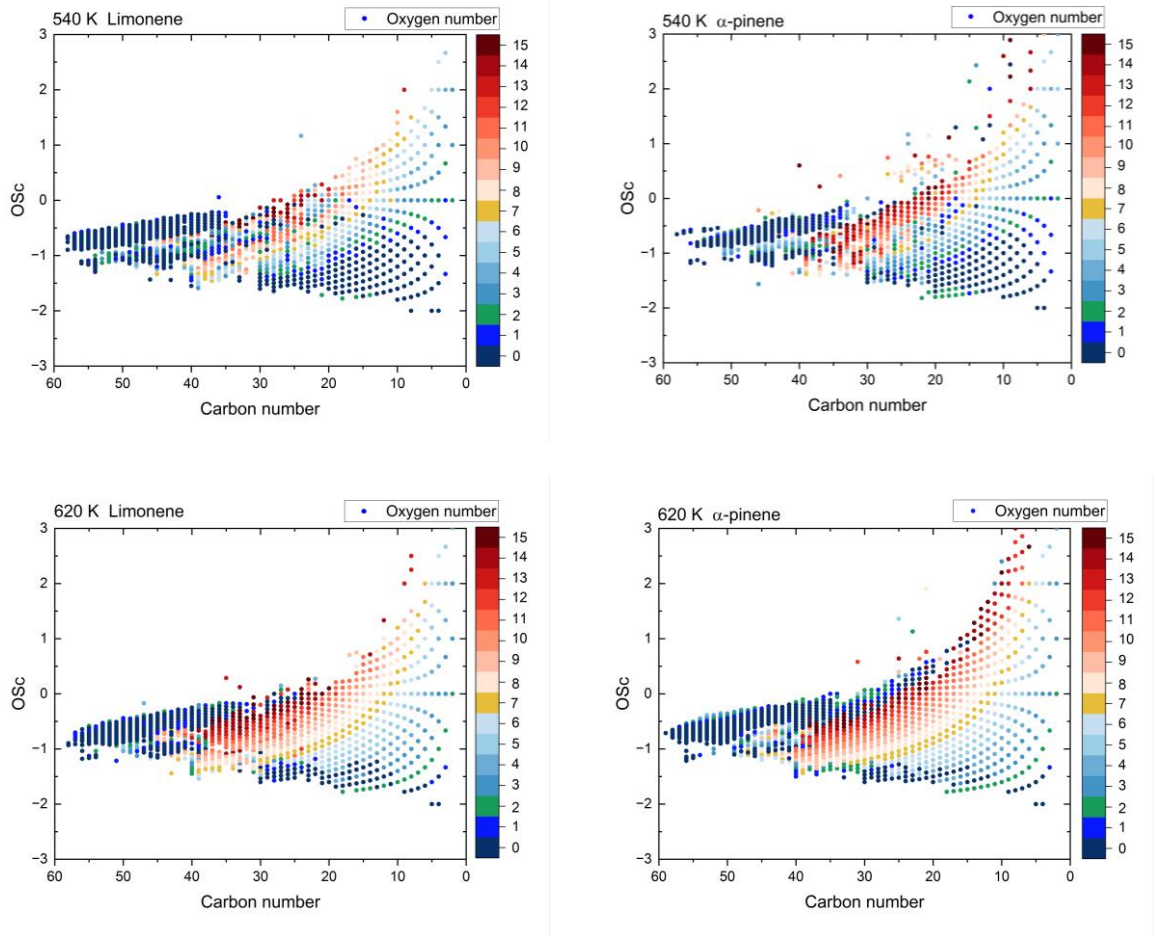

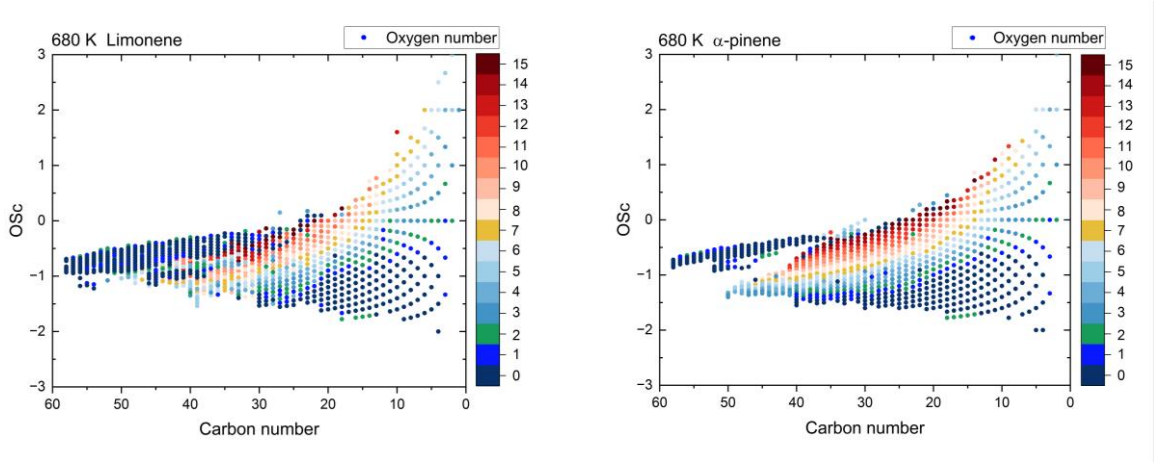


253 **Fig. 5.** Overview of the distribution of limonene (left) and α-pinene (right) oxidation products observed.
254 HESI+/–, FIA-HRMS data were used.

255 As can be seen from Fig. 5, similar trends were observed for both fuels. If we consider OSc ≥ 0 for
256 α-pinene, one can observe an increase of the number of chemical formulas between 540 and 620 K and
257 a decrease of that number at 680 K. Also, one can see that the content of oxygen in chemical formulas
258 is higher for α-pinene products at 620 K. This difference increases at 680 K, especially for chemical
259 compounds with carbon numbers between 20 and 30. The formation of dimers and trimers is probably
260 more developed in the case of limonene with carbon numbers close to 60 (see Fig. S9). The absence of
261 oxygen for OSc<0 and C>40 confirms the presence of unsaturated or aromatic chemical compounds, as
262 proposed elsewhere [36].

263

264 *3.2 Polyunsaturated or aromatic products of oxidation*

265

266 The formation of $C_nH_4$ (n=5-6), and $C_nH_6$ (n=6-9) isomers was observed for both terpene fuels on
267 the vertical line with O/C = 0 (line 4) in Van Krevelen plots using HESI+/– FIA-HRMS data (in Fig. 4;
268 the location of the fuels is shown as a circle). These plots indicated the formation of aromatics (H/C <
269 0.7 and O/C = 0) and polyunsaturated products. In the space defined by 0 < O/C < 0.2, we observed
270 products of oxidation (line 1) and dehydrogenation (line 4). For H/C <1, the degree of oxidation of
271 products decreases with the H/C ratio.

272 Plotting Van Krevelen diagram at different temperatures indicated some variations in several regions.
273 Indeed, when the temperature increases, for H/C <1 and O/C <0.1, many more chemical formulas were
274 detected. In particular, one could observe three subsets with 1 to 3 oxygen atoms which grow with
275 temperature up to 620 K (Figs. 6 and 7). At 680 K, we observed a clear decrease of the population of

chemical compounds containing 0, 1, 2 or 3 O-atom in the case of α-pinene. In this space of the VK diagram, these oxygen additions are not random, since more than 50% of the chemical formulas remain with the same number of carbon and hydrogen atoms. If we associate these observations with reaction paths, one could propose that the oxidation products contain OH groups or ether functions.

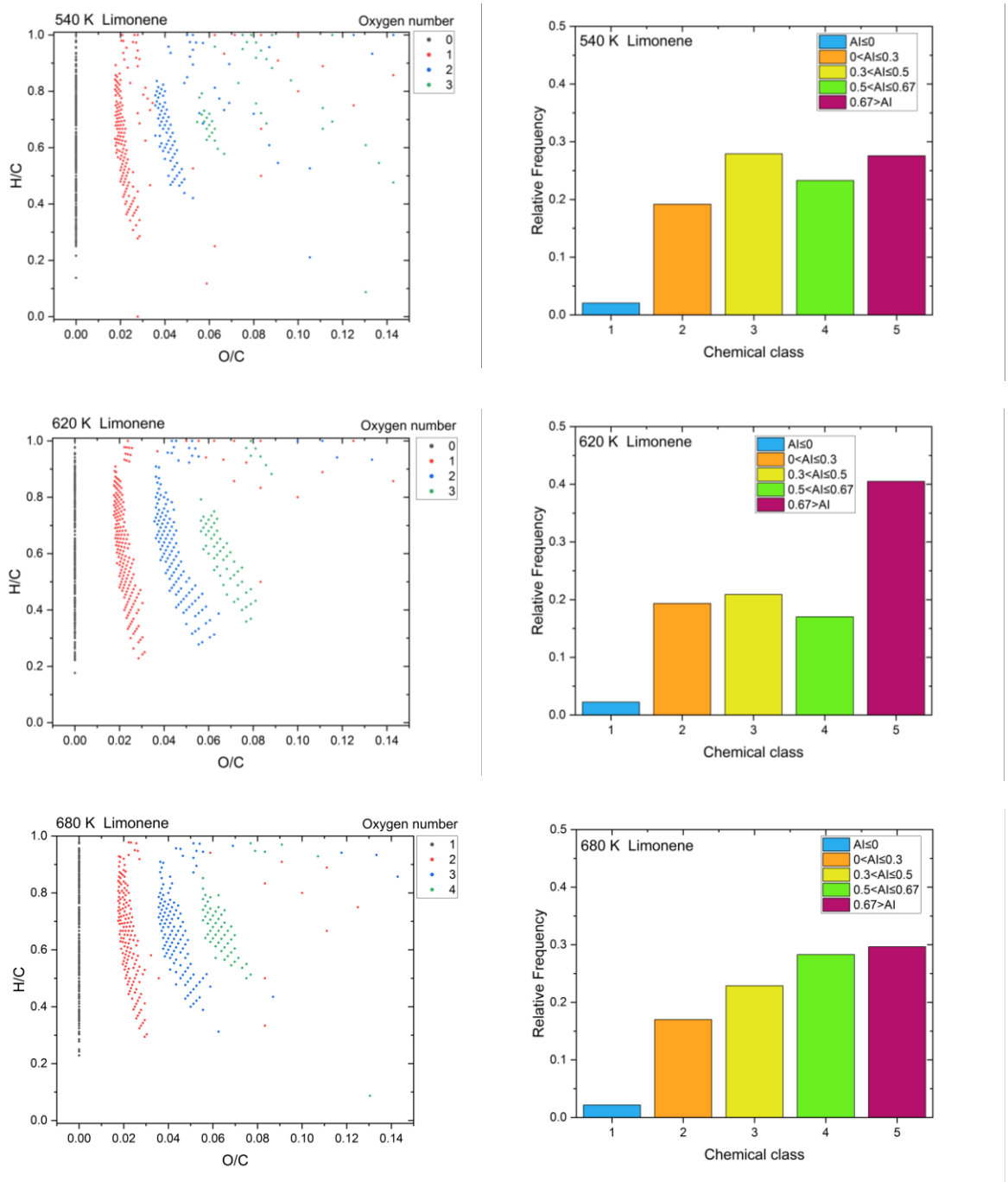


**Fig. 6.** Van Krevelen plot for limonene oxidation products at three different temperatures (left) and frequency of occurrence of chemical classes (right). HESI+/–, FIA-HRMS data were used.

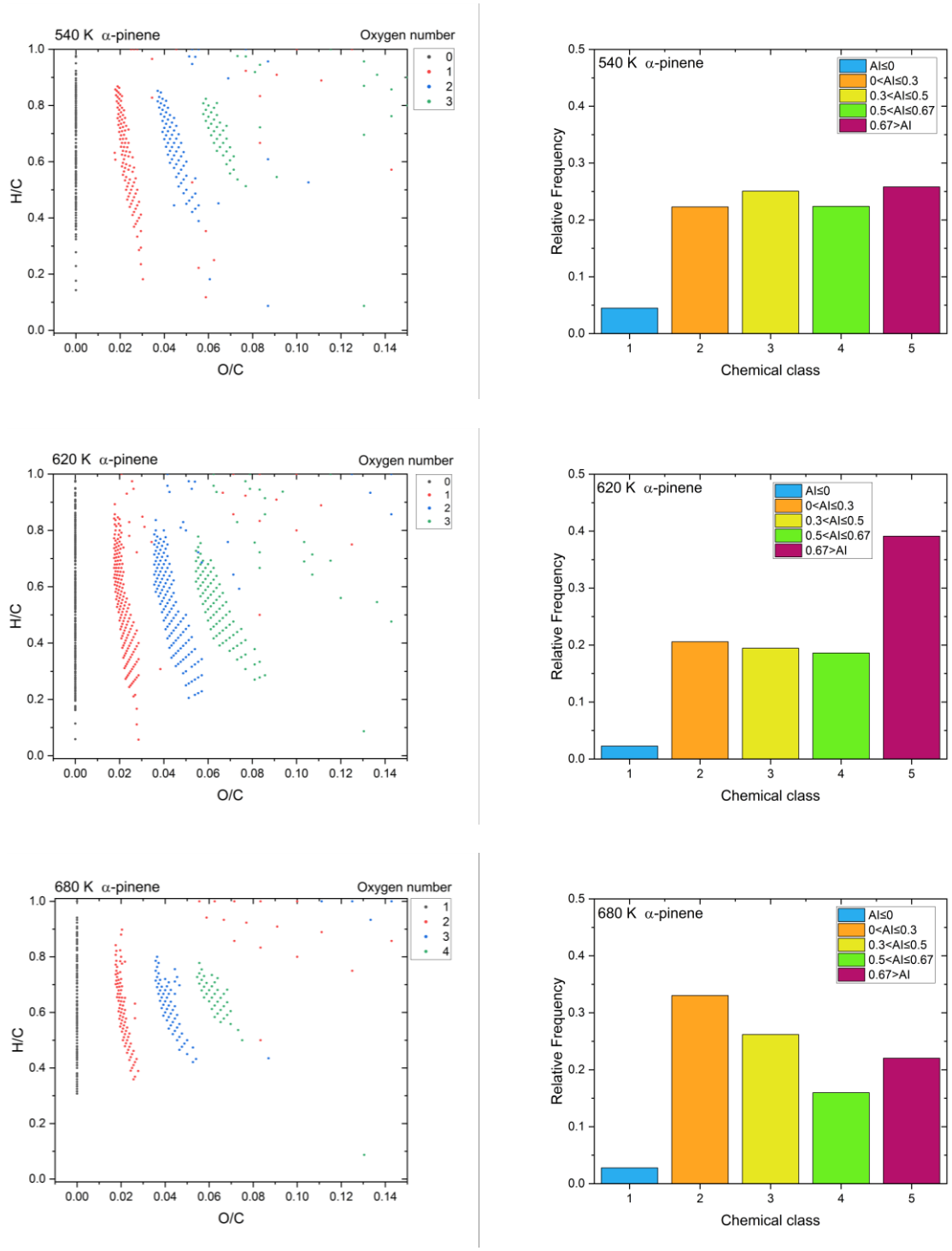


283 **Fig. 7.** Van Krevelen plot for α-pinene oxidation products at three different temperatures (left) and
284 frequency of occurrence of chemical classes (right). HESI+/–, FIA-HRMS.

285 In order to further assess the presence of different chemical classes in the products of oxidation of
286 the fuels, we computed the aromaticity index ($AI_{mod}$) and defined chemical families based on literature
287 [37]: (1) aliphatics ($AI_{mod} \leq 0$), (2) olefinics and naphtenics ($0 < AI_{mod} \leq 0.3$), (3) highly unsaturated

compounds ($0.3< AI_{mod} \leq 0.5$), (4) aromatics ($0.5< AI_{mod} \leq 0.67$), and (5) polyaromatics ($0.67< AI_{mod}$). One should note that the fuels have an $AI_{mod}$ of 0.3; then, they are included in class (2). Here, the AI was computed according to the equation: $AI_{mod} = (1 + C - 0.5\times O - 0.5\times H)/(C - 0.5\times O)$, where C, H, and O represent the number of carbon, hydrogen, and oxygen atoms, respectively, in the chemical formulas [19, 38]; see Figs. S7 and S8 for full dataset analysis. The differentiation of chemical classes of products arising from the oxidation of the two terpenes is particularly important at the early stages of oxidation. The histograms presented in Figs. 6 and 7 represent more than 1,000 chemical formulas detected in the subset $O/C \leq 0.1$ (1 to 3 additions of O) and $H/C \leq 1$. As can be seen from Figs. 6 and 7, for limonene and α-pinene, respectively, the aromatic fraction (4) decreases and the polyaromatic fraction (5) increases at 620 K. That could indicate an increased production of polyaromatic from aromatic products. However, at 680 K, these last two chemical classes decrease significantly in the case of α-pinene. In the case of limonene, for AI > 0.67 we observe chemical formulas with 40 to 60 carbon atoms which, given the unsaturation level, could correspond to chemicals with structural units composed of 3 to 4 aromatic rings. Beyond these hypotheses, we observed that for limonene (Fig. 6), chemical compounds with AI > 0.67 dominate at higher temperature (i.e., 680 K) which could be due to higher thermal stability, lower oxidation rates or higher production rates.

Whereas the computation of $AI_{mod}$ is useful for probing the presence of aromatics in oxidation products, computing the aromaticity equivalent index (Xc) is of greater value, according to previous works [20]. Therefore, Xc were computed for the oxidation products of limonene and α-pinene. Xc was defined as: $[3(DBE - m\times O) – 2] / (DBE - m\times O)$, with m=1, as in previous works [20]. In that paper, the authors classified the chemical formulas according to Xc ($Xc \geq 2.5$ for aromatics; $Xc \geq 2.7143$ for condensed aromatics). Figure 8 shows the present results. One can see that the formation of polyaromatics ($2.9 \leq Xc \leq 3$) is confirmed. One can also note that more aromatics were detected in α-pinene oxidation products.

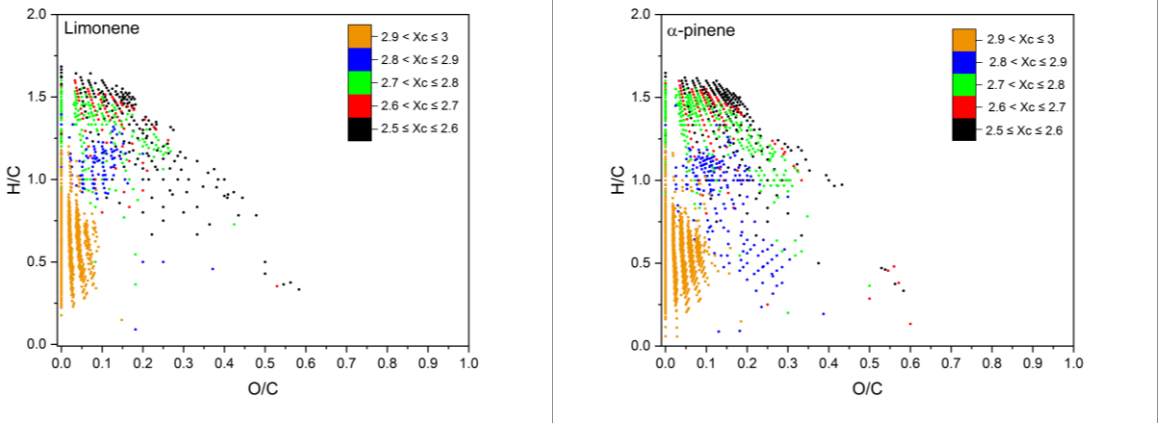


**Fig. 8.** Van Krevelen-Xc plot for limonene (left) and α-pinene (right) oxidation products. HESI+/–, FIA-

HRMS (samples taken at 620 K). The color-coding indicates the computed Xc values.

For $2.9 \leq Xc \leq 3$, we observed a carbon number distribution centered mainly on ~$C_{50}$, which is not the case for the multimodal distributions (~ 10, 20, 30, 40, 50, ... carbon atoms) observed during the formation of dimers, trimers or the initiation of oligomerization (Fig. S9). Finally, in the space $H/C \leq 1$ and $0 \leq O/C \leq 0.15$, where Xc is in the range 2.9 to 3, we detected 82-85 % of the total chemical formulas with HESI (–). Then considering that aromatics are easily ionized with HESI (–) [39, 40], one can conclude that aromatic products dominate in that space. Table S2 summarizes the detected formulas with $O/C = 0$ and $H/C < 0.7$. To date, no reaction mechanism is available to describe their formation, although one can speculate that they are formed via recombination reactions involving e.g., hydrocarbon radicals and hydrocarbons.

Whereas the presently observed formation of aromatics or polyunsaturated products under cool-flame conditions was rather unexpected, it should be investigated further since the oxidation of aromatics could significantly contribute to the formation of secondary organic aerosols in the troposphere [41].

## 4. Conclusions

In this study, we detected a large set of complex products of oxidation formed from cool flames of two monoterpenes, limonene and α-pinene, at atmospheric pressure and fuel-lean conditions. Oxidation pathways including autoxidation, the Waddington mechanism involving *exo*- and *endo*-double bonds (C=C), autoxidation of its products, and the Korcek mechanism. The formation of aromatic and polyunsaturated products was observed during the autoxidation of the two fuels through the use of HRMS combined with graphic tools (Van Krevelen plots, oxidation state of carbon, aromaticity index, and aromaticity equivalent index). The presence of unsaturated or polyunsaturated chemical compounds at these temperatures needs to be investigated further. This work demonstrates that oxidation pathways are numerous and complex, and many complex chemical products can be formed whereas reaction pathways need to be delineated. The oxidation products detected in this work can be emitted to the troposphere, which would increase the concentration of VOCs contributing to the formation of particulates. The present results could be useful to improve existing atmospheric models.

## Acknowledgements

Support from the CAPRYSSES project (ANR- 11-LABX-006–01) and the VOLTAIRE project (ANR-

10-LABX-100-01) funded by ANR through the PIA (Programme d'Investissement d'Avenir) is gratefully acknowledged.

## References


[1] Seinfeld, JH, Pandis, SN, Atmospheric Chemistry and Physics: From Air Pollution to Climate Change. 2nd ed.; Wiley-Interscience: Hoboken, NJ, 2006, p. 1232.

[2] Pourbafrani, M, Forgács, G, Horváth, IS, Niklasson, C, Taherzadeh, MJ, Production of biofuels, limonene and pectin from citrus wastes. Bioresour. Technol. 2010; 101: 4246-4250.

[3] Harvey, BG, Wright, ME, Quintana, RL, High-Density Renewable Fuels Based on the Selective Dimerization of Pinenes. Energy Fuels 2010; 24: 267-273.

[4] Musyaroh, Wijayanti, W, Sasongko, MN, Winarto, The role of limonene in the branching of straight chains in low-octane hydrocarbons. Renewable Energy 2023; 204: 421-431.

[5] Polikarpov, E, Albrecht, KO, Page, JP, Malhotra, D, Koech, PK, Cosimbescu, L, Gaspar, DJ, Critical fuel property evaluation for potential gasoline and diesel biofuel blendstocks with low sample volume availability. Fuel 2019; 238: 26-33.

[6] Berndt, T, Richters, S, Kaethner, R, Voigtländer, J, Stratmann, F, Sipilä, M, Kulmala, M, Herrmann, H, Gas-phase ozonolysis of cycloalkenes: formation of highly oxidized RO2 radicals and their reactions with NO, NO2, SO2, and other RO2 radicals. The Journal of Physical Chemistry A 2015; 119: 10336-10348.

[7] Chetehouna, K, Courty, L, Mounaim-Rousselle, C, Halter, F, Garo, J-P, Combustion Characteristics of p-Cymene Possibly Involved in Accelerating Forest Fires. Combust. Sci. Technol. 2013; 185: 1295-1305.

[8] Courty, L, Chetehouna, K, Halter, F, Foucher, F, Garo, JP, Mounaim-Rousselle, C, Experimental determination of emission and laminar burning speeds of alpha-pinene. Combust. Flame 2012; 159: 1385-1392.

[9] Bierkandt, T, Hoener, M, Gaiser, N, Hansen, N, Koehler, M, Kasper, T, Experimental flat flame study of monoterpenes: Insights into the combustion kinetics of alpha-pinene, beta-pinene, and myrcene. Proc. Combust. Inst. 2021; 38: 2431-2440.

[10] Morley, C, A Fundamentally Based Correlation Between Alkane Structure and Octane Number. Combust. Sci. Technol. 1987; 55: 115-123.

[11] Wang, Z, Popolan-Vaida, DM, Chen, B, Moshammer, K, Mohamed, SY, Wang, H, Sioud, S, Raji, MA, Kohse-Höinghaus, K, Hansen, N, Dagaut, P, Leone, SR, Sarathy, SM, Unraveling the structure and chemical mechanisms of highly oxygenated intermediates in oxidation of organic compounds. Proceedings of the National Academy of Sciences 2017; 114: 13102-13107.

[12] Wang, ZD, Chen, BJ, Moshammer, K, Popolan-Vaida, DM, Sioud, S, Shankar, VSB, Vuilleumier, D, Tao, T, Ruwe, L, Brauer, E, Hansen, N, Dagaut, P, Kohse-Hoinghaus, K, Raji, MA, Sarathy, SM, n-Heptane cool flame chemistry: Unraveling intermediate species measured in a stirred reactor and motored engine. Combust. Flame 2018; 187: 199-216.

[13] Ray, DJM, Redfearn, A, Waddington, DJ, Gas-phase oxidation of alkenes: decomposition of hydroxy-substituted peroxyl radicals. Journal of the Chemical Society, Perkin Transactions 2 1973; 540-543.

[14] Ranzi, E, Cavallotti, C, Cuoci, A, Frassoldati, A, Pelucchi, M, Faravelli, T, New reaction classes in the kinetic modeling of low temperature oxidation of n-alkanes. Combust. Flame 2015; 162: 1679-1691.

[15] Xie, C, Lailliau, M, Issayev, G, Xu, Q, Chen, W, Dagaut, P, Farooq, A, Sarathy, SM, Wei, L, Wang, Z, Revisiting low temperature oxidation chemistry of n-heptane. Combust. Flame 2022; 242: 112177.

[16] Dbouk, Z, Belhadj, N, Lailliau, M, Benoit, R, Dayma, G, Dagaut, P, Normal butane oxidation: Measurements of autoxidation products in a jet-stirred reactor. Fuel 2023; 350: 28865.

[17] Van Krevelen, DW, Graphical-statistical method for the study of structure and reaction processes of coal. Fuel 1950; 29: 269-284.

[18] Kroll, JH, Donahue, NM, Jimenez, JL, Kessler, SH, Canagaratna, MR, Wilson, KR, Altieri, KE, Mazzoleni, LR, Wozniak, AS, Bluhm, H, Mysak, ER, Smith, JD, Kolb, CE, Worsnop, DR, Carbon oxidation state as a metric for describing the chemistry of atmospheric organic aerosol. Nature Chemistry 2011; 3: 133-139.

[19] Koch, BP, Dittmar, T, From mass to structure: an aromaticity index for high-resolution mass data of natural organic matter. Rapid Commun. Mass Spectrom. 2016; 30: 250-250.

[20] Yassine, MM, Harir, M, Dabek-Zlotorzynska, E, Schmitt-Kopplin, P, Structural characterization of organic aerosol using Fourier transform ion cyclotron resonance mass spectrometry: Aromaticity equivalent approach. Rapid Commun. Mass Spectrom. 2014; 28: 2445-2454.

[21] Dagaut, P, Cathonnet, M, Rouan, JP, Foulatier, R, Quilgars, A, Boettner, JC, Gaillard, F, James, H, A jet-stirred reactor for kinetic studies of homogeneous gas-phase reactions at pressures up to ten atmospheres (≈1 MPa). Journal of Physics E: Scientific Instruments 1986; 19: 207-209.
[22] Dagaut, P, Cathonnet, M, Boettner, JC, Experimental-Study and Kinetic Modeling of Propene Oxidation in a Jet Stirred Flow Reactor. J. Phys. Chem. 1988; 92: 661-671.
[23] Belhadj, N, Benoit, R, Dagaut, P, Lailliau, M, Serinyel, Z, Dayma, G, Oxidation of di-n-propyl ether: Characterization of low-temperature products. Proc. Combust. Inst. 2021; 38: 337-344.
[24] Belhadj, N, Lailliau, M, Benoit, R, Dagaut, P, Towards a Comprehensive Characterization of the Low-Temperature Autoxidation of Di-n-Butyl Ether. Molecules 2021; 26: 7174.
[25] Hecht, ES, Scigelova, M, Eliuk, S, Makarov, A, in: Encyclopedia of Analytical Chemistry, pp 1-40.
[26] Hu, Z, Di, Q, Liu, B, Li, Y, He, Y, Zhu, Q, Xu, Q, Dagaut, P, Hansen, N, Sarathy, SM, Xing, L, Truhlar, DG, Wang, Z, Elucidating the photodissociation fingerprint and quantifying the determination of organic hydroperoxides in gas-phase autoxidation. Proceedings of the National Academy of Sciences 2023; 120: e2220131120.
[27] Belhadj, N, Benoit, R, Dagaut, P, Lailliau, M, Experimental characterization of n-heptane low-temperature oxidation products including keto-hydroperoxides and highly oxygenated organic molecules (HOMs). Combust. Flame 2021; 224: 83-93.
[28] Dbouk, Z, Belhadj, N, Lailliau, M, Benoit, R, Dagaut, P, Characterization of the Autoxidation of Terpenes at Elevated Temperature Using High-Resolution Mass Spectrometry: Formation of Ketohydroperoxides and Highly Oxidized Products from Limonene. J. Phys. Chem. A 2022; 126: 9087-9096.
[29] Witkowski, B, Al-Sharafi, M, Gierczak, T, Kinetics of Limonene Secondary Organic Aerosol Oxidation in the Aqueous Phase. Environmental Science & Technology 2018; 52: 11583-11590.
[30] St. John, PC, Guan, Y, Kim, Y, Kim, S, Paton, RS, Prediction of organic homolytic bond dissociation enthalpies at near chemical accuracy with sub-second computational cost. Nature Communications 2020; 11: 2328.
[31] St. John, PC, Guan, Y, Kim, Y, Etz, BD, Kim, S, Paton, RS, Quantum chemical calculations for over 200,000 organic radical species and 40,000 associated closed-shell molecules. Scientific Data 2020; 7: 244.
[32] Demarque, DP, Crotti, AEM, Vessecchi, R, Lopes, JLC, Lopes, NP, Fragmentation reactions using electrospray ionization mass spectrometry: an important tool for the structural elucidation and characterization of synthetic and natural products. Nat. Prod. Rep. 2016; 33: 432-455.
[33] Liang, Y, Simón-Manso, Y, Neta, P, Stein, SE, Unexpected Gas-Phase Nitrogen–Oxygen Smiles Rearrangement: Collision-Induced Dissociation of Deprotonated 2-(N-Methylanilino)ethanol and Morpholinylbenzoic Acid Derivatives. J. Am. Soc. Mass Spectrom. 2022; 33: 2120-2128.
[34] Kim, S, Kramer, RW, Hatcher, PG, Graphical Method for Analysis of Ultrahigh-Resolution Broadband Mass Spectra of Natural Organic Matter, the Van Krevelen Diagram. Anal. Chem. 2003; 75: 5336-5344.
[35] Bi, Y, Wang, G, Shi, Q, Xu, C, Gao, J, Compositional Changes during Hydrodeoxygenation of Biomass Pyrolysis Oil. Energy Fuels 2014; 28: 2571-2580.
[36] Wang, X, Hayeck, N, Brüggemann, M, Yao, L, Chen, H, Zhang, C, Emmelin, C, Chen, J, George, C, Wang, L, Chemical Characteristics of Organic Aerosols in Shanghai: A Study by Ultrahigh-Performance Liquid Chromatography Coupled With Orbitrap Mass Spectrometry. Journal of Geophysical Research: Atmospheres 2017; 122: 11,703-11,722.
[37] Schneider, E, Czech, H, Popovicheva, O, Lütdke, H, Schnelle-Kreis, J, Khodzher, T, Rüger, CP, Zimmermann, R, Molecular Characterization of Water-Soluble Aerosol Particle Extracts by Ultrahigh-Resolution Mass Spectrometry: Observation of Industrial Emissions and an Atmospherically Aged Wildfire Plume at Lake Baikal. ACS Earth and Space Chemistry 2022; 6: 1095-1107.
[38] Brege, MA, China, S, Schum, S, Zelenyuk, A, Mazzoleni, LR, Extreme Molecular Complexity Resulting in a Continuum of Carbonaceous Species in Biomass Burning Tar Balls from Wildfire Smoke. ACS Earth and Space Chemistry 2021; 5: 2729-2739.
[39] Shi, Z, Rao, Z, Zhao, J, Liang, M, Zhu, T, Wang, Y, Arandiyan, H, Target Screening of Hydroxylated and Nitrated Polycyclic Aromatic Hydrocarbons in Surface Water Using Orbitrap High-Resolution Mass Spectrometry in a Lake in Hebei, China. Separations 2021; 8: 247.
[40] Schneider, E, Giocastro, B, Rüger, CP, Adam, TW, Zimmermann, R, Detection of Polycyclic Aromatic Hydrocarbons in High Organic Carbon Ultrafine Particle Extracts by Electrospray Ionization Ultrahigh-Resolution Mass Spectrometry. J. Am. Soc. Mass Spectrom. 2022; 33: 2019-2023.
[41] Li, M, Li, J, Zhu, Y, Chen, J, Andreae, MO, Pöschl, U, Su, H, Kulmala, M, Chen, C, Cheng, Y, Zhao, J, Highly oxygenated organic molecules with high unsaturation formed upon photochemical aging of soot. Chem 2022; 8: 2688-2699.